Nanoscale

COMMUNICATION

View Article Online
View Journal | View Issue

Highly magnetic iron carbide nanoparticles as effective T_2 contrast agents†

Cite this: *Nanoscale*, 2014, **6**, 726

Received 3rd September 2013
Accepted 5th November 2013

DOI: 10.1039/c3nr04691e

www.rsc.org/nanoscale

Guoming Huang,[a] Juan Hu,[a] Hui Zhang,[a] Zijian Zhou,[a] Xiaoqin Chi[b] and Jinhao Gao*[a]

This paper reports that iron carbide nanoparticles with high air-stability and strong saturation magnetization can serve as effective T_2 contrast agents for magnetic resonance imaging. Fe_5C_2 nanoparticles (~20 nm in diameter) exhibit strong contrast enhancement with an r_2 value of 283.2 mM^{-1} S^{-1}, which is about twice as high as that of spherical Fe_3O_4 nanoparticles (~140.9 mM^{-1} S^{-1}). *In vivo* experiments demonstrate that Fe_5C_2 nanoparticles are able to produce much more significant MRI contrast enhancement than conventional Fe_3O_4 nanoparticles in living subjects, which holds great promise in biomedical applications.

Magnetic resonance imaging (MRI), based on the interaction of protons with the surrounding molecules of tissues that can provide excellent anatomical details, is currently one of the most powerful medical imaging techniques.[1] MRI contrast agents are a group of contrast media that can greatly improve the accuracy and specificity of MRI by enhancing the visibility of the target from the background.[2–5] For example, superparamagnetic iron oxide nanoparticles with the ability to shorten T_2 relaxation times are one of the most common negative contrast agents and have been used in the clinic.[6–8] However, iron oxide nanoparticles with relatively low saturation magnetization exhibit moderate T_2 contrast enhancement. The transverse relaxivity (r_2) values of commercial iron oxide based contrast agents, such as ferumoxides, ferumoxtran, and ferumoxsil, are typically in the range 50–110 mM^{-1} S^{-1} at 0.47 T.[9] Recently, intensive research has been devoted to synthesizing highly magnetic nanoparticles, since nanoparticles with larger saturation magnetizations can more effectively shorten T_2 relaxation times, resulting in greater MRI contrast enhancement.[10–12] For example, manganese or zinc-doped iron oxide nanoparticles with high magnetization and increased relaxivity have been developed.[13–16] However, doping nanoparticles with potentially toxic metals has always been a concern because of their harmful effects in living organisms. Iron has the highest saturation magnetization at room temperature of any element,[17] and has been shown to be a safe element in the body after the biodegradation of iron oxide nanoparticles,[18,19] suggesting that iron nanoparticles may be ideal contrast agents for high-performance MRI. Despite tremendous efforts, the development of stable iron nanoparticles remains challenging due to the fast oxidation of iron and the significant loss of magnetization upon exposure to air,[20] which hampers the further biomedical applications. Therefore, it is necessary to develop a suitable iron-based contrast agent that not only has a large saturation magnetization value, but also is stable in biological media for diagnostic applications.

Iron carbides have attracted considerable attention over the past several decades owing to their distinguished properties and promising applications. Recently, several studies have been focused on the synthesis of iron carbide nanostructures with controlled size and morphology.[21–24] Iron carbide nanoparticles exhibit excellent catalytic activity and high magnetization, and hold great promise for applications in catalysis and magnetic hyperthermia.[23,24] Herein, we investigate the stability of iron carbide nanoparticles with high saturation magnetization and report that Fe_5C_2 nanoparticles can serve as biocompatible and effective T_2 contrast agents for *in vivo* MRI.

The transmission electron microscopy (TEM) image shows that the as-synthesized Fe_5C_2 nanoparticles were ~20 nm in diameter with spherical and rod-shaped structures (Fig. 1a). The high-resolution TEM (HRTEM) image reveals that the lattice spacing in the core was 0.205 nm, corresponding to the (510) plane of Fe_5C_2, while the shell was amorphous (Fig. 1b). The X-ray powder diffraction (XRD) pattern confirms that the crystal structure of iron carbide nanoparticles is consistent with that of Fe_5C_2 (JCPDS no. 36-1248). We further employed X-ray photoelectron spectroscopy (XPS) to investigate the surface

[a]*State Key Laboratory of Physical Chemistry of Solid Surfaces, The Key Laboratory for Chemical Biology of Fujian Province and Department of Chemical Biology, College of Chemistry and Chemical Engineering, Xiamen University, Xiamen 361005, China. E-mail: jhgao@xmu.edu.cn; Fax: +86-592-2189959; Tel: +86-592-2180278*

[b]*Fujian Provincial Key Laboratory of Chronic Liver Disease and Hepatocellular Carcinoma, Zhongshan Hospital, Xiamen University, Xiamen 361004, China*

† Electronic supplementary information (ESI) available: Supplementary figures and experimental details. See DOI: 10.1039/c3nr04691e

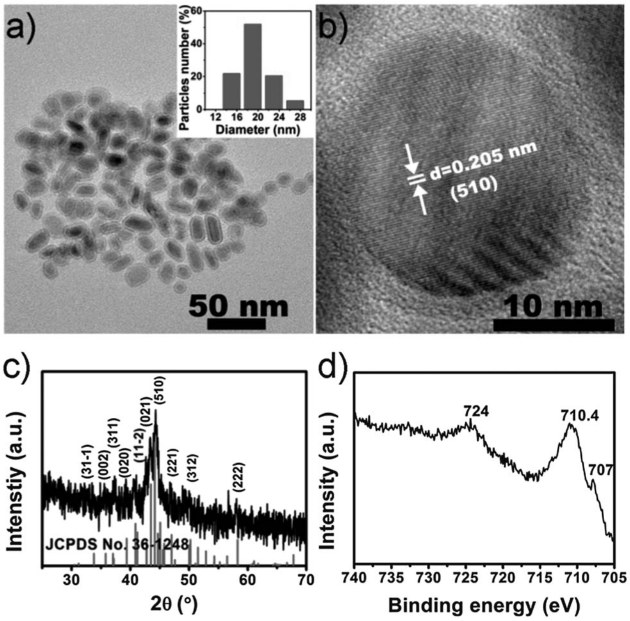

Fig. 1 (a) TEM image and size distribution histogram (inset), (b) HRTEM image, (c) XRD pattern, and (d) Fe 2p XPS spectrum of Fe_5C_2 nanoparticles.

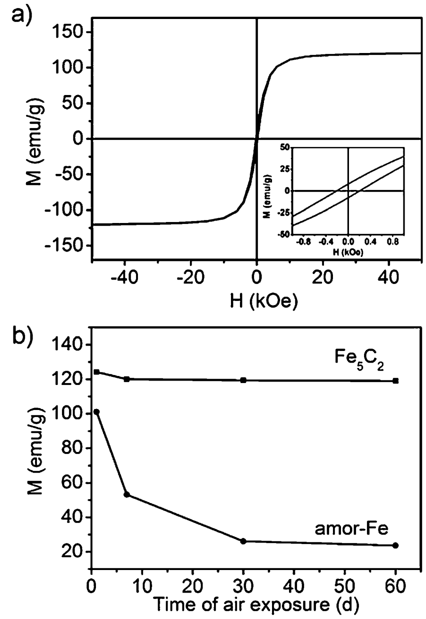

Fig. 2 (a) Magnetic hysteresis loop of the Fe_5C_2 nanoparticles recorded at 300 K (inset: magnification of the low-field region). (b) Stability analysis of Fe_5C_2 nanoparticles and amor-Fe nanoparticles in air.

nature of Fe_5C_2 nanoparticles (Fig. 1d). The peak at ~707 eV in the Fe 2p XPS spectrum can be ascribed to the Fe–C bond,[23] indicating the successful synthesis of iron carbide nanoparticles. Two peaks at ~710.4 eV and ~724 eV can be assigned to iron(III) oxide,[25] together with the peak at ~284 eV in the C 1s spectrum (Fig. S1†), indicating the coexistence of the iron oxide and the carbon amorphous shell.[23]

We then investigated the magnetic properties of Fe_5C_2 nanoparticles using a superconducting quantum interference device (SQUID) magnetometer. The hysteresis loop shows that the as-synthesized Fe_5C_2 nanoparticles exhibit a soft ferro/ferrimagnetic behavior with a saturation magnetization value of ~120 emu g^{-1} at 300 K (Fig. 2a). This saturation magnetization value is very close to that of the iron carbides reported previously,[22,26] and is much higher than that of iron oxide nanoparticles with similar size (typically range from 40–70 emu g^{-1}).[27–29] Remarkably, the Fe_5C_2 nanoparticles also display a high stability against oxidation. The Fe_5C_2 nanoparticles show little magnetization change even after two month air exposure (Fig. 2b). The highly crystalline structure and the presence of carbon atoms may prevent the oxidation of Fe_5C_2 nanoparticles. For comparison, we synthesized the amorphous Fe (denoted as amor-Fe) nanoparticles[20] with ~14 nm in diameter and studied the stability in air. The saturation magnetization of the freshly prepared ~10 nm Fe nanoparticles has been reported up to 198 emu g^{-1}.[24] In our experiment, the saturation magnetization of the as-synthesized ~14 nm amor-Fe nanoparticles dropped to ~100 emu g^{-1} only after 1 day air exposure, and was further decreased to ~26 emu g^{-1} after 30 days. Obviously, the Fe_5C_2 nanoparticles are much more stable than amor-Fe nanoparticles in air, suggesting that Fe_5C_2 nanoparticles with great feature of excellent oxidation resistance are suitable for further potential applications.

To make the as-synthesized Fe_5C_2 nanoparticles water-dispersible for biomedical applications, we simply modified the particle surface with sodium tartrate *via* a ligand exchange method. The obtained aqueous solution containing Fe_5C_2 nanoparticles is highly stable over at least three months without any precipitate (Fig. S2†), suggesting that tartrate-coated Fe_5C_2 nanoparticles are suitable for *in vitro* and *in vivo* studies. The morphology of nanoparticles shows no obvious change as observed in TEM images (Fig. S2†). The dynamic light scattering (DLS) analysis indicates that the tartrate-coated Fe_5C_2 nanoparticles are very stable without aggregation in aqueous solution (Fig. S3†). We then evaluated the cytotoxicity of the water-dispersible Fe_5C_2 nanoparticles using the tetrazolium-based colorimetric assay (MTT assay). The result shows that more than 85% of cells were viable even at the highest concentration (100 μg Fe mL^{-1}, ~1.8 mM, measured by inductively coupled plasma atomic emission spectroscopy, ICP-AES), indicating the good biocompatibility of tartrate-coated Fe_5C_2 nanoparticles (Fig. 3).

We next investigated the ability of Fe_5C_2 nanoparticles for MRI contrast enhancement. We used Fe_3O_4 nanoparticles (~20 nm in diameter) and amor-Fe nanoparticles (~14 nm in diameter) as two control samples (Fig. S4†). All tartrate-coated solution samples have been stored in the air for one month. We first prepared samples of these three types of nanoparticles with different Fe concentrations (determined by ICP-AES) and collected the T_2-weighted phantom images at a 0.5 T MRI system. For a given Fe concentration, Fe_5C_2 nanoparticles exhibit the strongest negative contrast effect (darken signal) among three types of nanoparticles, suggesting the capability of Fe_5C_2 nanoparticles as high-performance T_2 MRI contrast agents (Fig. 4a). We further measured the transverse relaxivity (r_2) at 0.5 T according to the linear relationship of transverse

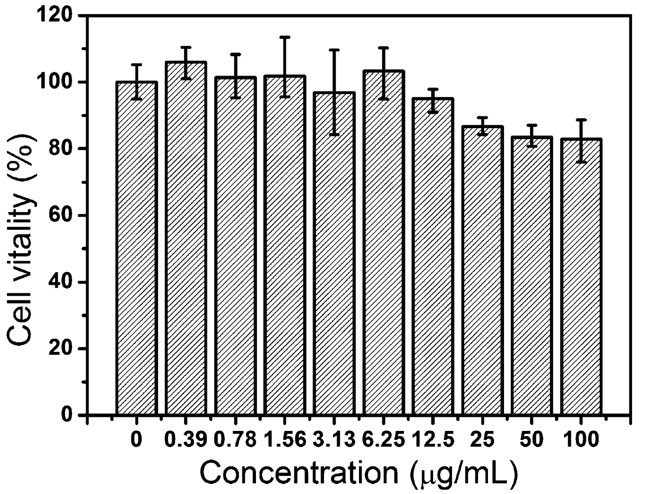

Fig. 3 Cell viability of HeLa cells after being incubated with Fe_5C_2 nanoparticles with different Fe concentrations at 37 °C for 24 h.

relaxation rates (R_2, *i.e.*, $1/T_2$) *versus* Fe concentrations (Fig. 4b). The r_2 value of Fe_5C_2 nanoparticles is $\sim$283.2 mM^{-1} S^{-1}, which is about twice as high as that of Fe_3O_4 nanoparticles ($\sim$140.9 mM^{-1} S^{-1}) and also much higher than those of commercial T_2 contrast agents (*e.g.*, ferumoxides),[9] confirming that Fe_5C_2 nanoparticles have much stronger T_2 contrast enhancement than Fe_3O_4 nanoparticles. On the basis of the quantum mechanical outer sphere theory, the T_2 relaxivity is highly dependent on the saturation magnetization of the nanoparticles.[12,30,31] Fe_5C_2 nanoparticles with high saturation magnetization can afford effective magnetic relaxations to the water protons around the nanoparticles and therefore results in the enhanced relaxivity.[32,33] The r_2 value of amor-Fe nanoparticles is only 12.7 mM^{-1} S^{-1}, which is extremely lower than those of Fe_5C_2 nanoparticles and Fe_3O_4 nanoparticles. The significant loss of magnetization results in the poor performance of amor-Fe nanoparticles in MRI contrast enhancement. Moreover, the further oxidation and instability of amor-Fe nanoparticles make them unsuitable for biomedical applications. Thus, we only used Fe_5C_2 nanoparticles and Fe_3O_4 nanoparticles as samples in subsequent *in vivo* MRI experiments.

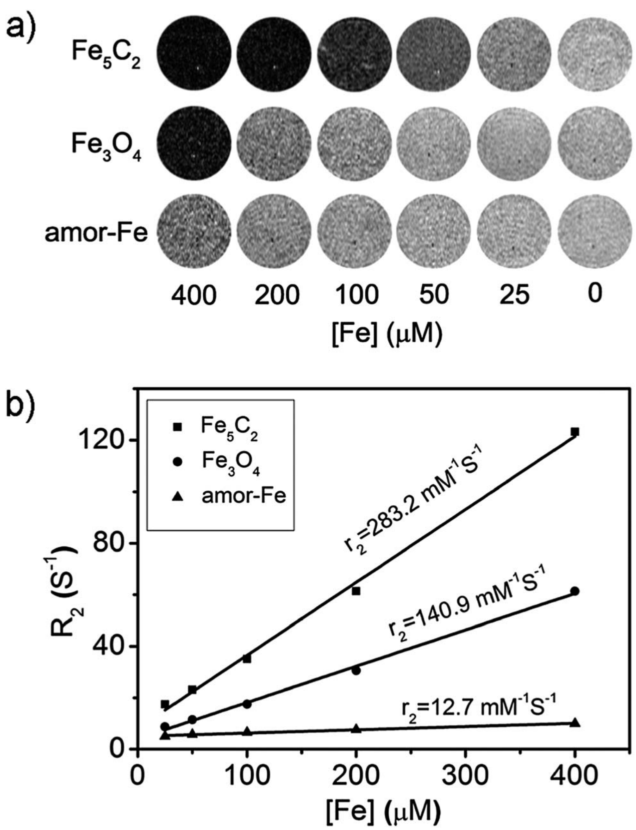

Fig. 4 (a) T_2-weighted phantom images of Fe_5C_2 nanoparticles, Fe_3O_4 nanoparticles, and amor-Fe nanoparticles in aqueous solution (containing 1% agar) with different Fe concentrations, respectively. (b) The linear fitting of relaxation rates (R_2) *versus* Fe concentrations for Fe_5C_2 nanoparticles, Fe_3O_4 nanoparticles, and amor-Fe nanoparticles, respectively. The relaxivity values (r_2) were obtained from the slopes.

Iron oxide nanoparticles have been extensively developed for the diagnosis of liver diseases because they are highly taken up by the hepatic Kupffer cells.[34–36] Thus, we focused on the liver as the targeting region for evaluating the *in vivo* MRI effects of Fe_5C_2 nanoparticles. The r_2 values of the Fe_5C_2 and Fe_3O_4 nanoparticles are 428.5 and 232.2 mM^{-1} S^{-1} at 7 T, respectively (Fig. S5†). Meanwhile, the r_2 value of Fe_5C_2 nanoparticles is approximately two times larger than that of Fe_3O_4 nanoparticles, which is consistent with the results obtained at 0.5 T. We intravenously injected Fe_5C_2 nanoparticles and Fe_3O_4 nanoparticles into the BALB/c mice (dosage of 2.0 mg Fe per kg, Fe concentration determined by ICP-AES) and obtained T_2-weighted images at different time points after injection on a 7 T Varian MRI scanner. Fe_5C_2 nanoparticles and Fe_3O_4 nanoparticles may have comparable biodistribution (*e.g.*, similar liver uptake of nanoparticles) because of their similar size and surface chemistry.[37,38] Both coronal and transverse images show that the liver regions exhibited a noticeably darker signal after the injection of Fe_3O_4 and Fe_5C_2 nanoparticles (Fig. 5a and S6†). In comparison with Fe_3O_4 nanoparticles, Fe_5C_2 nanoparticles produced significantly darker signal in liver regions probably due to their higher r_2 value. To quantify the contrast enhancement, we calculated the signal-to-noise ratio (SNR) by finely analyzing regions of interest (ROIs) of the transverse images and defined the contrast enhancement as the decrease of SNR, $\triangle SNR = (|SNR_{post} - SNR_{pre}|)/SNR_{pre}$. The measured $\triangle$SNR values of the Fe_5C_2 nanoparticle group are 54.1 ± 7.3%, 68.8 ± 5.4%, 85.0 ± 3.8%, 58.8 ± 7.7% at 0.5, 1 h, 2 h, 4 h after the injection, respectively, which is much higher than those of the Fe_3O_4 nanoparticle group (26.8 ± 3.4%, 43.7 ± 3.2%, 47.1 ± 1.7%, and 27.9 ± 3.0%, respectively), further demonstrating the excellent contrast ability of Fe_5C_2 nanoparticles in MRI of small living subjects (Fig. 5b). It is worth noting that the $\triangle$SNR values have been falling at 4 h, and further decrease to 28.2 ± 5.4% and 15.3 ± 2.2% 24 h after the injection of Fe_5C_2 and Fe_3O_4 nanoparticles, respectively. It is necessary to conduct MRI scanning within 2–4 h after administration of Fe_5C_2 nanoparticles, which also meets the basic requirements of clinical diagnosis.

In summary, we successfully synthesized Fe_5C_2 nanoparticles and investigated their ability to serve as high-performance T_2

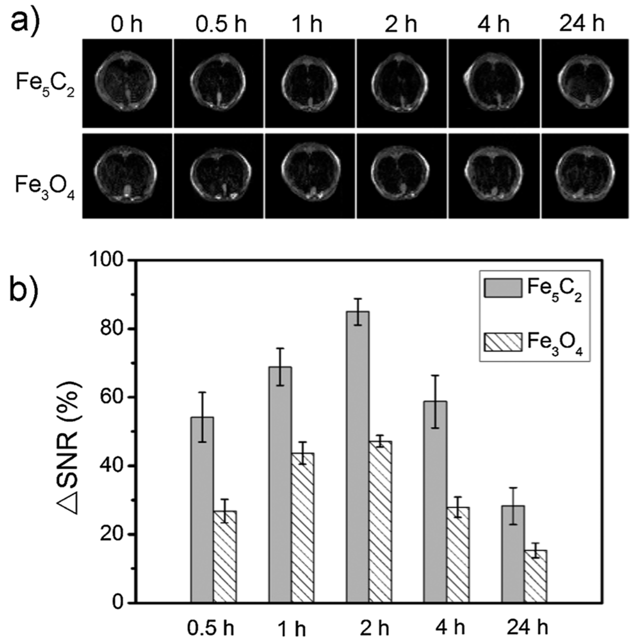

Fig. 5 (a) T_2-weighted *in vivo* MRI images of mice (transverse plane) collected at different time points after intravenous injection of Fe_5C_2 nanoparticles and Fe_3O_4 nanoparticles (with a dose of 2.0 mg Fe per kg of mouse body weight), respectively. (b) The decrease of signal-to-noise ratio (△SNR) at different time points after intravenous injection of Fe_5C_2 nanoparticles and Fe_3O_4 nanoparticles ($n = 3$), respectively.

contrast agents. The as-synthesized 20 nm Fe_5C_2 nanoparticles have a high saturation magnetization (~120 emu g^{-1}) and remarkable oxidation resistance. Both *in vitro* and *in vivo* studies demonstrated that the Fe_5C_2 nanoparticles were able to effectively shorten T_2 relaxation times (with an r_2 value of 283.2 mM^{-1} S^{-1} at 0.5 T) and produce significant MRI contrast enhancement. We believe that such highly magnetic and stable iron carbide nanoparticles hold great promise in serving as novel and effective MRI contrast agents for liver imaging.

This work was supported by the National Key Basic Research Program of China (2013CB933901 and 2014CB744502), National Natural Science Foundation of China (21222106, 81370042, 81000662, and 81201805), Natural Science Foundation of Fujian (2013J06005), and Program for New Century Excellent Talents in University (NCET-10-0709).

Notes and references

1 Z. P. Liang and P. C. Orth, *Principles of Magnetic Resonance Imaging: A Signal Processing Perspective*, Wiley-IEEE Press, 1999.
2 D. Ho, X. Sun and S. Sun, *Acc. Chem. Res.*, 2011, **44**, 875–882.
3 C. Tassa, S. Y. Shaw and R. Weissleder, *Acc. Chem. Res.*, 2011, **44**, 842–852.
4 J. H. Gao, H. W. Gu and B. Xu, *Acc. Chem. Res.*, 2009, **42**, 1097–1107.
5 F. Q. Hu, H. M. Joshi, V. P. Dravid and T. J. Meade, *Nanoscale*, 2010, **2**, 1884–1891.
6 H. B. Na, I. C. Song and T. Hyeon, *Adv. Mater.*, 2009, **21**, 2133–2148.
7 S. Laurent, D. Forge, M. Port, A. Roch, C. Robic, L. Vander Elst and R. N. Muller, *Chem. Rev.*, 2008, **108**, 2064–2110.
8 R. Qiao, C. Yang and M. Gao, *J. Mater. Chem.*, 2009, **19**, 6274–6293.
9 C. W. Jung and P. Jacobs, *Magn. Reson. Imaging*, 1995, **13**, 661–674.
10 Y. W. Jun, J. H. Lee and J. Cheon, *Angew. Chem., Int. Ed.*, 2008, **47**, 5122–5135.
11 Y. W. Jun, J. W. Seo and J. Cheon, *Acc. Chem. Res.*, 2008, **41**, 179–189.
12 D. Yoo, J. H. Lee, T. H. Shin and J. Cheon, *Acc. Chem. Res.*, 2011, **44**, 863–874.
13 S. H. Sun, H. Zeng, D. B. Robinson, S. Raoux, P. M. Rice, S. X. Wang and G. X. Li, *J. Am. Chem. Soc.*, 2004, **126**, 273–279.
14 J. H. Lee, Y. M. Huh, Y. W. Jun, J. W. Seo, J. T. Jang, H. T. Song, S. Kim, E. J. Cho, H. G. Yoon, J. S. Suh and J. Cheon, *Nat. Med.*, 2007, **13**, 95–99.
15 T. J. Yoon, H. Lee, H. Shao and R. Weissleder, *Angew. Chem., Int. Ed.*, 2011, **50**, 4663–4666.
16 J. T. Jang, H. Nah, J. H. Lee, S. H. Moon, M. G. Kim and J. Cheon, *Angew. Chem., Int. Ed.*, 2009, **48**, 1234–1238.
17 D. L. Huber, *Small*, 2005, **1**, 482–501.
18 M. Levy, N. Luciani, D. Alloyeau, D. Elgrabli, V. Deveaux, C. Pechoux, S. Chat, G. Wang, N. Vats, F. Gendron, C. Factor, S. Lotersztajn, A. Luciani, C. Wilhelm and F. Gazeau, *Biomaterials*, 2011, **32**, 3988–3999.
19 J. D. Lopez-Castro, A. V. Maraloiu, J. J. Delgado, J. J. Calvino, M. G. Blanchin, N. Galvez and J. M. Dominguez-Vera, *Nanoscale*, 2011, **3**, 4597–4599.
20 S. Peng, C. Wang, J. Xie and S. Sun, *J. Am. Chem. Soc.*, 2006, **128**, 10676–10677.
21 C. Giordano, A. Kraupner, S. C. Wimbush and M. Antonietti, *Small*, 2010, **6**, 1859–1862.
22 Z. Schnepp, S. C. Wimbush, M. Antonietti and C. Giordano, *Chem. Mater.*, 2010, **22**, 5340–5344.
23 C. Yang, H. Zhao, Y. Hou and D. Ma, *J. Am. Chem. Soc.*, 2012, **134**, 15814–15821.
24 A. Meffre, B. Mehdaoui, V. Kelsen, P. F. Fazzini, J. Carrey, S. Lachaize, M. Respaud and B. Chaudret, *Nano Lett.*, 2012, **12**, 4722–4728.
25 J. F. Moulder, W. F. Stickle, P. E. Sobol and K. D. Bomben, *Handbook of X-ray photoelectron spectroscopy*, Perkin-Elmer Corporation, Physical Electronics Division, Eden Prairie, MN, USA, 1992.
26 L. J. E. Hofer and E. M. Cohn, *J. Am. Chem. Soc.*, 1959, **81**, 1576–1582.
27 K. Woo, J. Hong, S. Choi, H.-W. Lee, J.-P. Ahn, C. S. Kim and S. W. Lee, *Chem. Mater.*, 2004, **16**, 2814–2818.
28 J. Park, K. An, Y. Hwang, J. G. Park, H. J. Noh, J. Y. Kim, J. H. Park, N. M. Hwang and T. Hyeon, *Nat. Mater.*, 2004, **3**, 891–895.
29 C. Hui, C. Shen, T. Yang, L. Bao, J. Tian, H. Ding, C. Li and H. J. Gao, *J. Phys. Chem. C*, 2008, **112**, 11336–11339.
30 A. Roch, R. N. Muller and P. Gillis, *J. Chem. Phys.*, 1999, **110**, 5403–5411.

31 Z. Zhao, Z. Zhou, J. Bao, Z. Wang, J. Hu, X. Chi, K. Ni, R. Wang, X. Chen, Z. Chen and J. Gao, *Nat. Commun.*, 2013, **4**, 2266.
32 S. H. Koenig and K. E. Kellar, *Magn. Reson. Med.*, 1995, **34**, 227–233.
33 A. J. Villaraza, A. Bumb and M. W. Brechbiel, *Chem. Rev.*, 2010, **110**, 2921–2959.
34 S. Mornet, S. Vasseur, F. Grasset and E. Duguet, *J. Mater. Chem.*, 2004, **14**, 2161–2175.
35 J. Huang, L. H. Bu, J. Xie, K. Chen, Z. Cheng, X. G. Li and X. Y. Chen, *ACS Nano*, 2010, **4**, 7151–7160.
36 Z. Zhou, D. Huang, J. Bao, Q. Chen, G. Liu, Z. Chen, X. Chen and J. Gao, *Adv. Mater.*, 2012, **24**, 6223–6228.
37 A. Albanese, P. S. Tang and W. C. Chan, *Annu. Rev. Biomed. Eng.*, 2012, **14**, 1–16.
38 Z. Zhou, L. Wang, X. Chi, J. Bao, L. Yang, W. Zhao, Z. Chen, X. Wang, X. Chen and J. Gao, *ACS Nano*, 2013, **7**, 3287–3296.